Biosensors and Bioelectronics 59 (2014) 384–388

Contents lists available at ScienceDirect

Biosensors and Bioelectronics

journal homepage: www.elsevier.com/locate/bios

Short communication

3D graphene foams decorated by CuO nanoflowers for ultrasensitive ascorbic acid detection

Ye Ma [a], Minggang Zhao [a], Bin Cai [a], Wei Wang [a], Zhizhen Ye [a,b], Jingyun Huang [a,b,*]

[a] State Key Laboratory of Silicon Materials, Department of Materials Science and Engineering, Zhejiang University, Hangzhou 310027, China
[b] Cyrus Tang Center for Sensor Materials and Applications, Zhejiang University, Hangzhou 310058, China

ARTICLE INFO

Article history:
Received 2 January 2014
Received in revised form
14 March 2014
Accepted 31 March 2014
Available online 13 April 2014

Keywords:
Three dimensions
Graphene foam
Free-standing
Copper oxide
Ascorbic acid
Biosensor

ABSTRACT

When the in vitro research works of biosensing begin to mimic in vivo conditions, some certain three-dimensional (3D) structures of biosensors are needed to accommodate biomolecules, bacteria or even cells to resemble the in vivo 3D environment. To meet this end, a novel method of synthesizing CuO nanoflowers on the 3D graphene foam (GF) was first demonstrated. The 3DGF/CuO nanoflowers composite was used as a monolithic free-standing 3D biosensor for electrochemical detection of ascorbic acid (AA). The 3D conductive structure of the GF is favorable for current collection, mass transport and loading bioactive chemicals. And CuO nanoflowers further increase the active surface area and catalyze the redox of AA. Thus, all these features endows 3DGF/CuO composite with outstanding biosensing properties such as an ultrahigh sensitivity of 2.06 mA mM^{-1} cm^{-2} to AA at 3 s response time.

1. Introduction

Cells, bacteria and many other microbes are inherently sensitive to local macroscale, microscale and nanoscale three-dimensional (3D) environment and the adherence to a 3D structure is often needed (da Rocha-Azevedo and Grinnell, 2013; Muller et al., 2013). With the advancements of in vitro research of biomolecule detections, drug delivery, tissue culture and microbial fuel cells, researchers begin to focus on mimicking the in vivo condition to make sure that their results are still reliable when applied to the in vivo process of bio-metabolism (Nirantar et al., 2013; Rawson et al., 2013; Zhao et al., 2013). It would be more attractive to associate the level of analytes in the solution with the quantity and health condition of cells and bacteria all by one integrated biosensor. Therefore, a 3D structure is essential for designing the new generation biosensors. But the traditional biosensors are mostly 1D or 2D devices that the electrocatalytic materials are often attached to an inactive electrode to detect the analytes and cannot be easily shaped into three dimensions (Wang, 2008) to support bioactive molecules. Meanwhile, the traditional scaffolds can provide a bio-friendly 3D morphology but cannot provide sufficient feedbacks concerning the level of analytes due to the poor conductivity of scaffolds (Grafahrend et al., 2011). So a bioactive 3D biosensor is expected to meet both the needs.

Graphene, a two-dimensional monolayer of sp2 carbon atoms, has drawn numerous interest in this decade owning to its large specific surface area, unusual mechanical strength, outstanding electrical properties and good bio-compatibility (Reina et al., 2008; Tao et al., 2013; Zhang et al., 2013b). In particular, many research works have focused on graphene-based materials for high-performance biosensors (Pumera, 2011; Sun et al., 2011b; Wu et al., 2013; Yang et al., 2010). However, the conventional grown graphene is always a two-dimensional sheet and its morphology cannot be easily changed which limits the active surface area and further applications (Huang et al., 2011). Therefore, three-dimensional graphene foams (3DGF), a seamlessly connected porous carbon network can desirably tackle these problems to be an ideal conductive scaffold to replace the traditional supporting electrodes.

Ascorbic acid (AA), also known as vitamin C is a common water soluble pharmaceutical compound usually used to prevent or treat some diseases in public. AA is vital to many human metabolism processes such as enhancing iron uptake in human intestinal cells, involving in immune cell functions and immune responses and inducing differentiation of cells (Kim et al., 2012; Temu et al., 2010). Besides, bacteria also have close relationship with AA in food production and even the AA production itself (Dave and Shah, 1997). So a simple and rapid detection method of AA under complex condition is needed for biomedical chemistry, diagnostics and pathological research.

CuO, a transition metal oxide is under tremendous attention as biosensing materials due to their low cost, ease of synthesis, chemical stability and outstanding redox behavior at various

* Corresponding author.
E-mail address: huangjy@zju.edu.cn (J. Huang).

http://dx.doi.org/10.1016/j.bios.2014.03.064
0956-5663/

potential ranges under diverse reaction conditions. So CuO has been widely used as catalysis, semiconductors, gas sensors and Li-ion rechargeable batteries (Dubal et al., 2013; Steinhauer et al., 2013; Sun et al., 2013). Some previous studies have shown that CuO has notable electrochemical properties of catalyzing biomolecules, therefore predict direct electrochemical detection of AA without the need of any other mediators (Hsu et al., 2012; Jiang and Zhang, 2010; Jindal et al., 2012). Moreover, the variable nanostructures of CuO could further enlarge the specific surface area and the quantity of active sites to obtain impressive sensitivity.

In this study, we demonstrate a 3DGF/CuO nanoflowers composite as a novel free-standing and monolithic biosensor with large specific surface area, high conductive pathways, well-organized 3D porous structure and ultrahigh sensitivity for AA. The 3D morphology and high sensitivity make it a promising biosensor for in vitro detection mimicking in vivo condition in the future.

2. Experimental

2.1. Fabrication of 3D graphene foam

As described in previous study (Chen et al., 2011), the 3DGF was synthesized by CVD on 1.5 mm × 1 cm × 1 cm nickel foam under atmosphere pressure. The samples were first heated to 1000 °C with the flow of H_2 and Ar (H_2/Ar=150:300 sccm). Then 15 sccm CH_4 was introduced into the quartz tube to synthesize the graphene in 15 min. After the growth, samples were rapidly cooled down to room temperature in 10 min with the protection of H_2 and Ar. At last, the Ni/GF were immersed into 3 M HCl solution at 80 °C to etch away the nickel foam to get the free-standing 3DGF.

2.2. Synthesis of 3D graphene and CuO nanoflowers composite

First, the Cu nanoparticles were electrodeposited on the 3D graphene foam by maintaining potential −0.40 V for 30 s in 0.1 M H_2SO_4, 0.01 M $CuSO_4$ solution. The samples served as the working electrode in a three-electrode system. Then the sample was immersed into a solution of 0.05 M $K_2S_2O_8$, 1.5 M NaOH at 80 °C for 5 min to get the final 3DGF/CuO nanoflowers composite.

2.3. Synthesis of CuO electrode

Similar to the synthesis of 3DGF/CuO nanoflowers, Cu nanoparticles were electrodeposited on the glass carbon electrode (GCE, diameter 3 mm) then oxidized into CuO nanoflowers.

2.4. Characterization

The morphology of samples was characterized with HITACHI S-4800 electron microscopy (SEM). Energy-dispersive X-ray spectroscopy (EDX) was tested by EDAX Gernesis. Raman spectra were recorded at ambient temperature on a Labor Raman HR-800 system with 514.532 nm wavelength laser. The X-ray diffraction (XRD) was carried out on a PANalytical B.V. Empyrean 200895 (Netherland) using Cu Kα radiation.

2.5. Electrochemical measurements

The electrochemical impedance spectroscopy (EIS) was performed with CHI 760e (U.S.). The other electrochemical experiments were carried out with a WPG100e electrochemical workstation (Korea). A three-electrode system was employed in all electrochemical experiments. Rinsed by ethanol and water twice, the 3DGF or 3DGF/CuO were griped by a Pt clip which is connected to the electrochemical workstation. The 3DGF or 3DGF/CuO composite served as the working electrode, while a platinum electrode and a SCE electrode were used as the counter and reference electrodes, respectively.

3. Results and discussion

3.1. Characterization of 3DGF/CuO

As shown in Fig. 1a, the as prepared 3DGF/CuO composite is much darker than the 3DGF in color, indicating that the CuO nanoflowers have been evenly anchored on the surface of 3DGF. The structure and morphology are then studied by scanning electron microscopy (SEM, Fig. 1b–f). The bare 3DGF is a smooth and macro-porous graphene skeleton with wrinkles distributed on the surface (Fig. 1b). The hollow graphene bridge is about 50 μm wide with no cracks or breaks and the diameter of pores ranges from 100 μm to 300 μm. As to the 3DGF/CuO composite, Fig. 1c–f show that the 3DGF is uniformly covered by CuO nanoflowers which is about 400 nm in diameter with thin nanoflakes (about 10 nm thick, 50 nm wide and 200 nm long) as petals (Fig. 1f). The 3DGF provides an ideal morphology for anchoring bioactive molecules and rapid pathway for mass transfer, while CuO nanoflowers offer a large accessible surface area and numerous chemical active sites.

The XRD pattern is shown in Fig. 1g. All peaks can be assigned to either 3DGF or CuO, which shows no impurity phase exists and good crystallinity of CuO. The Raman spectra of graphene foam (Fig. 1h) show two characteristic peaks at 1581 cm^{-1} and 2725 cm^{-1} which can be attributed to G and 2D peaks. No peaks at 1350 cm^{-1} indicate good quality and the lack of defects (Malard et al., 2009). The elemental purity of the 3DGF/CuO composite was also confirmed by EDX (Fig. 1h inset), showing only C, O, and Cu in the sample.

3.2. Electrochemical properties

First, the electrochemical active surface areas (ECSA) of CuO/GCE, 3DGF and 3DGF/CuO were calculated as 0.0861 cm^2, 3.99 cm^2 and 8.98 cm^2, according to the Randles–Sevcik equation (Lu et al., 2008):

$$I_p = 268600\, n^{2/3} A D^{1/2} C v^{1/2}$$

where I_p is current maximum in amps, n number of electrons transferred in the redox event, A the electrochemical active area in cm^2, D diffusion coefficient in cm^2/s (6.70×10^{-6} cm^2/s), C concentration in mol/L (0.005 M $K_3Fe(CN)_6$) and v scan rate in V/s. The relative standard deviation (R.S.D.) of ECSA among three 3DGF/CuO sensors is 5.7%. The merit that 3DGF/CuO has the largest ECSA promises its good biosensing property.

The electrochemical properties of 3DGF/CuO composite were then examined by EIS in 0.1 M phosphate buffer solution (PBS, pH 7.4) in the frequency range from 0.1 Hz to 100 kHz. As shown in the Nyquist plots (Fig. 2a), the resistance of 3DGF/CuO (20 Ω) is much smaller than that of bare 3DGF (28 Ω) and CuO on GCE (157 Ω) in the high frequency domain, indicating that the 3DGF/CuO has higher electrochemical activity and faster electron transfers on the surface than the bare 3DGF and CuO (Wang et al., 2010).

Fig. 2b shows the different cyclic voltammetry (CV) response of CuO on GCE, the bare 3DGF and 3DGF/CuO in 40 μM AA and 0.1 M phosphate buffer solution at the scan rate of 50 mV/s from −0.8 V to 0.4 V. The dramatically enhanced CV curve of 3DGF/CuO indicates the high electrocatalytic activity of CuO nanoflowers comparing with the bare 3DGF electrode and fast charge collecting

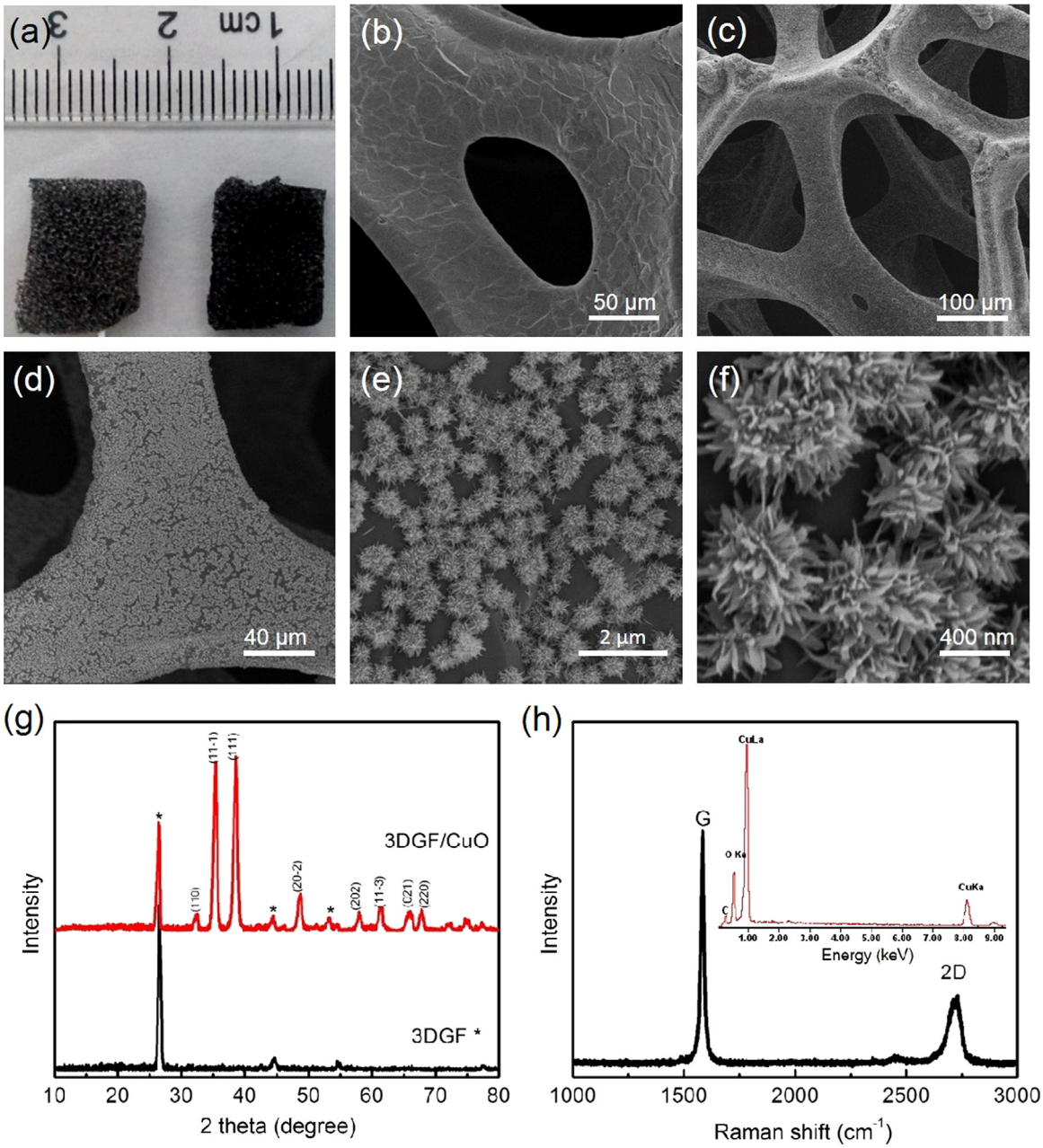

Fig. 1. Morphology, phase and elemental purity of 3DGF and 3DGF/CuO composite. (a) Photographs of 3DGF on the left and 3DGF/CuO composite on the right showing that CuO nanoflowers have blacken the surface of 3DGF. (b) SEM image of 3DGF surface; (c–f) Low-to high-magnification SEM images of 3DGF/CuO nanoflowers composite. (g) XRD patterns of 3DGF and 3DGF/CuO composite. (h) Raman spectra of 3DGF and inset shows the EDS of 3DGF/CuO composite.

property comparing with CuO/GCE. Furthermore, a negative potential shift of the onset of the oxidation peak can be observed from −0.1 V of 3DGF to −0.15 V of 3DGF/CuO composite, which indicates the 3DGF/CuO composite can reduce the overpotential in AA oxidation. Since the AA oxidation is an inner-sphere reaction that is sensitive to the surface of electrode (Wu et al., 2012), the vast number of active sites provided by CuO nanoflowers on the 3DGF can lower the energy barrier of AA redox and act as a media to boost electron transfer between AA in the solution and the 3DGF. When the scan rate increases, both the current and the potential of the oxidation peak increase (Fig. 2c), and the anodic peak current is proportional to the square root of the scan rate ($V^{1/2}$, Fig. 2c inset). The linear relationship between I_{peak} and $V^{1/2}$ is I_{peak} (mA)=0.589 $V^{1/2}$ −0.783 (R=0.999), suggesting the redox reaction of AA is controlled by the mass transfer process (Dong et al., 2012). Therefore, it highlights the key role of the 3D structure of graphene skeleton that provides an ideal morphology for anchoring bioactive molecules and rapid pathway for mass transfer. When 40 μM AA is introduced into 0.1 M PBS, the anodic peak at about 0.2 V is greatly enhanced (Fig. 2d) which corresponds with previous study (Wen et al., 2010), suggesting the best detecting potential of AA.

3.3. Ascorbic acid sensing

Holding the potential of the oxidation peak at 0.2 V in 0.1 M PBS with the AA concentration ranged from 0 to 240 μM, the corresponding calibration curve of current versus AA concentration is plotted in Fig. 2e. An ultrahigh sensitivity of 2.06 mA mM^{-1} cm^{-2} is achieved and the linear range is up to 200 μM (R=0.994). Besides, the response time is as short as 3 s and lowest detection limit can be calculated as 430 nM (S/N=3). The comparison of amperometric responses among CuO, 3DGF and 3DGF/CuO is also studied in Fig. 2e

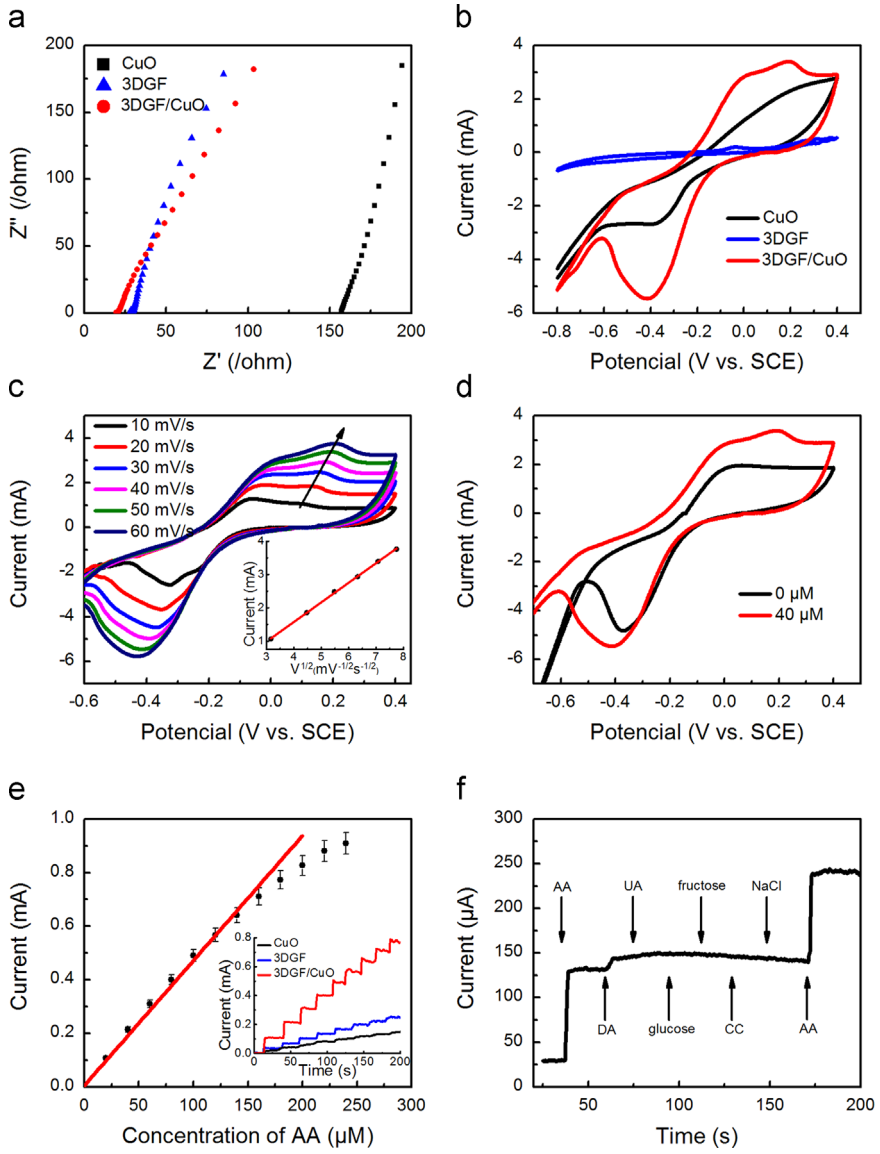

Fig. 2. Electrochemical performance and AA sensing of 3DGF and 3DGF/CuO in 0.1 M PBS (pH 7.4). (a) Nyquist plots of CuO, 3DGF and 3DGF/CuO composite electrodes in the frequency range from 0.1 Hz to 100 kHz. (b) CV curves of CuO, 3DGF and 3DGF/CuO composite in 40 μM AA solution with a scan rate of 50 mV. (c) CV curves of 3DGF/CuO composite at different scan rates (10, 20, 30, 40, 50 and 60 mV/s) in 40 μM AA solution. Inset is the plot of anodic peak current versus $V^{1/2}$. (d) CV curves 3DGF/CuO composite in 0 and 40 μM AA solution at the scan rate of 50 mV/s. (e) Dose response curve of 3DGF/CuO composite at the potential of 0.2 V, with a linear fitting at lower concentration range. The inset show the amperometric responses of CuO, 3DGF, and 3DGF/CuO composite toward successive addition of 20 μM AA per time at 0.2 V. (f) Amperometric response to the addition of 20 μM different analytes in the sequence of AA, dopamine (DA), uric acid (UA), glucose, fructose, choline chloride (CC), NaCl and AA.

inset. Obviously, the combination of 3DGF and CuO nanoflowers greatly augments the amperometric response to AA. And the R.S.D. of sensitivity among 6 samples is 4.4%. Furthermore, the 3DGF/CuO composite has good specificity to AA and can evade the interference of uric acid, glucose, fructose, choline chloride and NaCl and the interference of dopamine is as low as ~11% which suggest a potential for practical use (Fig. 2f). The comparison of analytical performance of the proposed 3DGF/CuO sensor with other published AA sensors are shown in Table 1. Although it does not have the widest linear range, the 3DGF/CuO composite possesses the highest sensitivity which is several fold to most reported AA sensors and very low detection limit. It should also be noted that some of graphene-based materials biosensors can simultaneously detect more than one analytes (Du et al., 2014; Ping et al., 2012). So the 3DGF/CuO composite could be a potential biosensing platform.

The whole oxidation process of AA can be described as this. First, the AA molecules in the solution are diffused to the nearest active sites on the 3DGF and are absorbed onto the petals of CuO nanoflowers. Then the surface absorbed AA molecules are oxidized to dehydroascorbic acid catalyzed by the conversion from CuO to Cu_2OOA on the surface: $(4CuO)_{surface}+C_6H_8O_6$ (ascorbic acid)$+2A^+ \rightarrow (2Cu_2OOA)_{surface}+C_6H_6O_6$ (dehydroascorbic acid)$+2H^+$, where A^+ can be either H^+ or Na^+ ion (Dubal et al., 2013).

The macropores of 3DGF can act as a bulk buffering reservoir for AA and other eletrolytes to minimize the diffusion distance of AA to the surface of CuO nanoflowers (Sattarahmady et al., 2013), which play a key role on preliminary stage of AA oxidation and result in the fast sensing responses. Moreover, due to its outstanding conductivity in three dimensions, the 3DGF also serves as a current collector to boost the current responses of AA oxidation

Table 1
Comparison of analytical performance of our proposed 3DGF/CuO sensor with other published AA sensors.

Electrode material	Linear range (μM)	Detection limit (μM)	Sensitivity (μA mM^{-1} cm^{-2})	Reference
GCE/MWCNT–Polyhis	250–2500	0.76	537	Dalmasso et al. (2012)
Pd nanowire modified GCE	250–900	0.2	166.5	Wen et al. (2010)
Graphene/Pt-modified GCE	0.15–34.4	0.15	1761.5	Sun et al. (2011a)
Ni–Pt alloys	570–5680	570	333	Weng et al. (2011)
F3O4/GO sheets	160–7200	20	33.5	Teymourian et al. (2013)
CuZEA/RGO/GCE	20–200	11	~430	He et al. (2012)
Screen-printed graphene	4–4500	0.95	392.5	Ping et al. (2012)
Gr flowers modified CF	45.4–1489.23	24.7	164	Du et al. (2014)
PdNi/C modified GCE	10–1800	0.5	760.6	Zhang et al. (2013a)
OPPy–PdNPs/Au	1–520	1	570	Shi et al. (2012)
3DGF/CuO nanoflowers	0.43–200	0.43	2060	Current work

(Ye et al., 2013), which induce the ultrahigh sensitivity of the 3DGF/CuO composite. Therefore, the 3DGF provides not only vast area for launching bioactive chemicals in a 3D manner, but also a highly conductive macro-porous network to enhance mass and electron transport to the CuO.

Meanwhile, CuO nanoflowers further enhance the response of AA sensing. Before the oxidation, AA molecules should first be absorbed onto the surface of the active sites (Li et al., 2013; Wu et al., 2013). So the radial petals of CuO nanoflowers maximize the accessible surface area to accommodate and catalyze AA molecules. Due to the high electrochemical and electrocatalytic properties, the CuO nanoflowers dominate the process of AA oxidation and function both as electrochemical active sites to boost the oxidation of AA and as an electron transfer media between the 3DGF and AA absorbed on the CuO surface. All these features indicate an excellent synergistic combination of 3DGF and CuO nanoflowers with ultrahigh sensitivity and fast response.

4. Conclusions

In conclusion, we demonstrate a facile synthesis route to produce a 3DGF and CuO nanoflowers composite employing CVD growth of graphene foam and electrochemistry synthesis of CuO nanoflowers. The 3DGF has outstanding mechanical strength and light weight to serve as a monolithic freestanding biosensing platform, and CuO nanoflowers show high crystallinity, uniform morphology and notable electrocatalytic properties. The combination of these two novel materials provide excellent synergistic biosensing properties, such as an ultrahigh sensitivity of 2.06 mA mM^{-1} cm^{-2} to AA, 3 s response time, low detecting limit and excellent specificity to AA. The 3D structure of GF is favorable for current collection, mass transport and loading bioactive chemicals. Meanwhile CuO nanoflowers further increase the active surface area and catalyze the redox of AA. It is expected that the unique hierarchical structure of 3DGF/CuO composite would be used not only as a real-time biosensor to detect analytes, but also as the a smart 3D bioactive platform supporting and monitoring cells or bacteria living condition in the in vitro or even in vivo research.

Acknowledgment

This work was supported by the Doctorate Fund of the Ministry of Education under Grant no. 2011010110013, the Innovation team of Zhejiang Province no. 2010R50020 and Ministry of Education of China IRT13037.

References

Chen, Z., Ren, W., Gao, L., Liu, B., Pei, S., Cheng, H., 2011. Nat. Mater. 10, 424–428.
da Rocha-Azevedo, B., Grinnell, F., 2013. Exp. Cell Res. 319, 2440–2446.
Dalmasso, P.R., Pedano, M.L., Rivas, G.A., 2012. Sens. Actuators B: Chem. 173, 732–736.
Dave, R.I., Shah, N.P., 1997. Int. Dairy J. 7, 435–443.
Dong, X., Wang, X., Wang, L., Song, H., Zhang, H., Huang, W., Chen, P., 2012. ACS Appl. Mater. Interfaces 4, 3129–3133.
Du, J., Yue, R., Ren, F., Yao, Z., Jiang, F., Yang, P., Du, Y., 2014. Biosens. Bioelectron. 53, 220–224.
Dubal, D.P., Gund, G.S., Holze, R., Lokhande, C.D., 2013. J. Power Sources 242, 687–698.
Grafahrend, D., Heffels, K.H., Beer, M.V., Gasteier, P., Moller, M., Boehm, G., Dalton, P. D., Groll, J., 2011. Nat. Mater. 10, 67–73.
He, P., Wang, W., Du, L., Dong, F., Deng, Y., Zhang, T., 2012. Anal. Chim. Acta 739, 25–30.
Hsu, Y.W., Hsu, T.K., Sun, C.L., Nien, Y.T., Pu, N.W., Ger, M.D., 2012. Electrochim. Acta 82, 152–157.
Huang, X., Yin, Z., Wu, S., Qi, X., He, Q., Zhang, Q., Yan, Q., Boey, F., Zhang, H., 2011. Small 7, 1876–1902.
Jiang, L., Zhang, W., 2010. Biosens. Bioelectron. 25, 1402–1407.
Jindal, K., Tomar, M., Gupta, V., 2012. Biosens. Bioelectron. 38, 11–18.
Kim, J.E., Cho, H.S., Yang, H.S., Jung, D.J., Hong, S.W., Hung, C.F., Lee, W.J., Kim, D., 2012. Immunobiology 217, 873–881.
Li, Y.C., Huang, F.Y., Chen, J., Mo, T., Li, S.X., Wang, F., Feng, S.Q., Li, Y.J., 2013. Int. J. Electrochem. Sci. 8, 6332–6342.
Lu, J., Do, I., Drzal, L.T., Worden, R.M., Lee, I., 2008. Acs Nano 2, 1825–1832.
Malard, L.M., Pimenta, M.A., Dresselhaus, G., Dresselhaus, M.S., 2009. Phys. Rep. 473, 51–87.
Muller, D., Silva, J.P., Rambo, C.R., Barra, G.M.O., Dourado, F., Gama, F.M., 2013. J. Biomater. Sci.-Polym. Ed. 24, 1368–1377.
Nirantar, S.R., Yeo, K.S., Chee, S., Lane, D.P., Ghadessy, F.J., 2013. Biosens. Bioelectron. 47, 421–428.
Ping, J., Wu, J., Wang, Y., Ying, Y., 2012. Biosens. Bioelectron. 34, 70–76.
Pumera, M., 2011. Mater. Today 14, 308–315.
Rawson, F.J., Yeung, C.L., Jackson, S.K., Mendes, P.M., 2013. Nano Lett. 13, 1–8.
Reina, A., Jia, X., Ho, J., Nezich, D., Son, H., Bulovic, V., Dresselhaus, M.S., Kong, J., 2008. Nano Lett. 9, 30–35.
Sattarahmady, N., Heli, H., Vais, R.D., 2013. Biosens. Bioelectron. 48, 197–202.
Shi, W., Liu, C., Song, Y., Lin, N., Zhou, S., Cai, X., 2012. Biosens. Bioelectron. 38, 100–106.
Steinhauer, S., Brunet, E., Maier, T., Mutinati, G.C., Kock, A., Freudenberg, O., Gspan, C., Grogger, W., Neuhold, A., Resel, R., 2013. Sens. Actuators B-Chem. 187, 50–57.
Sun, C., Lee, H., Yang, J., Wu, C., 2011a. Biosens. Bioelectron. 26, 3450–3455.
Sun, C.L., Chang, C.T., Lee, H.H., Zhou, J.G., Wang, J., Sham, T.K., Pong, W.F., 2011b. ACS Nano 5, 7788–7795.
Sun, C.L., Cheng, W.L., Hsu, T.K., Chang, C.W., Chang, J.L., Zen, J.M., 2013. Electrochem. Commun. 30, 91–94.
Tao, Y., Lin, Y., Ren, J., Qu, X., 2013. Biomaterials 34, 4810–4817.
Temu, T.M., Wu, K.Y., Gruppuso, P.A., Phornphutkul, C., 2010. Am. J. Physiol.-Endocrinol. Metab. 299, E325–E334.
Teymourian, H., Salimi, A., Khezrian, S., 2013. Biosens. Bioelectron. 49, 1–8.
Wang, J., 2008. Chem. Rev. 108, 814–825.
Wang, X., Hu, C., Liu, H., Du, G., He, X., Xi, Y., 2010. Sens. Actuators B: Chem. 144, 220–225.
Wen, D., Guo, S., Dong, S., Wang, E., 2010. Biosens. Bioelectron. 26, 1056–1061.
Weng, Y.-C., Lee, Y.-G., Hsiao, Y.-L., Lin, C.-Y., 2011. Electrochim. Acta 56, 9937–9945.
Wu, G., Wu, Y., Liu, X., Rong, M., Chen, X., Chen, X., 2012. Anal. Chim. Acta 745, 33–37.
Wu, S.X., He, Q.Y., Tan, C.L., Wang, Y.D., Zhang, H., 2013. Small 9, 1160–1172.
Yang, W.R., Ratinac, K.R., Ringer, S.P., Thordarson, P., Gooding, J.J., Braet, F., 2010. Angew. Chem.-Int. Ed. 49, 2114–2138.
Ye, S.B., Feng, J.C., Wu, P.Y., 2013. ACS Appl. Mater. Interfaces 5, 7122–7129.